Article

Correlating Acid Properties and Catalytic Function: A First-Principles Analysis of Alcohol Dehydration Pathways on Polyoxometalates

Michael J. Janik, Josef Macht, Enrique Iglesia, and Matthew Neurock

J. Phys. Chem. C, **2009**, 113 (5), 1872-1885• DOI: 10.1021/jp8078748 • Publication Date (Web): 07 January 2009

Correlating Acid Properties and Catalytic Function: A First-Principles Analysis of Alcohol Dehydration Pathways on Polyoxometalates

Michael J. Janik,[†] Josef Macht,[‡] Enrique Iglesia,[‡] and Matthew Neurock*[,§]

Departments of Chemical Engineering and Chemistry, University of Virginia, Charlottesville, Virginia 22904, Department of Chemical Engineering, Pennsylvania State University, University Park, Pennsylvania 16802, and Department of Chemical Engineering, University of California at Berkeley, Berkeley, California 94720

Received: September 04, 2008; Revised Manuscript Received: November 11, 2008

Density functional theory calculations and reactivity data were used to examine the mechanism of alcohol dehydration on Keggin-type polyoxometalate (POM) catalysts and the influence of the POM composition and the degree of substitution of the alcohol on kinetically relevant elimination steps. Dehydration was found to proceed through E1 pathways in which the alcohol C—O bond is cleaved heterolytically via a carbenium-ion transition state. Dehydration rates were found to depend on the elimination rate constant and the equilibrium constant for the formation of unreactive alcohol dimers. E2-type elimination transition states, involving concerted C—H and C—O bond cleavage, were not found. The extent of substitution at the α-carbon on the alcohol was found to lead to marked effects on elimination barriers, because substitution increases the proton affinity of the alcohol and the stability of the carbenium-ion transition state. Changes in the central and addenda atoms of the POM cluster and the presence of n-donors, a support, vicinal POM clusters, or charge-compensating cations were found to lead to changes in the deprotonation energy (DPE) of the POM cluster, activation barriers to dehydration, and the stability of the unreactive dimer. These effects are all captured in a general linear relation between activation barriers and deprotonation energy, a rigorous measure of acid strength. The explicit dependence of the E1 activation barrier on the acid deprotonation energy is much weaker than that on reactant proton affinity. This results from the more effective compensation between the acid deprotonation energy and the interaction energy between the cationic hydrocarbon fragment and the anionic POM cluster at the transition state. The direct interactions between the POM protons and the support, other POM clusters, n-donors, base probe molecules, and charge-compensating cations increased the negative charge of the oxide shell of the $W_{12}O_{40}$ conjugate base, which increased the DPE and decreased the POM acid strength. This decrease in acidity is not fully compensated by the concomitant increase in the interaction energy, leading to elimination barriers that generally increase with increasing DPE.

1. Introduction

The catalytic properties of solid acids are thought to reflect their intrinsic acid properties and, specifically, their experimentally elusive acid strengths. As such, a wide range of experimental methods, including titration with Hammett indicators,[1] temperature-programmed desorption of adsorbed base molecules,[1] adsorption microcalorimetry,[1−3] and ^{1}H NMR spectroscopy,[1−3] have been used to provide important information, although they incompletely describe the relevant features of solid acids. These methods cannot quantitatively probe intrinsic Brønsted acid strength and, as such, have made it difficult to develop fundamental structure−reactivity relationships.

A rigorous and catalytically relevant measure of Brønsted acid strength requires that one assesses the free energy required to remove a proton from the acid and stabilize the resulting anionic and cationic charges that form on the catalyst and the protonated reactant, respectively, in the ensuing ion pair. In the absence of direct measurements, theory, closely coupled with experiments, can provide reliable energies for each of these interactions and, thus, a quantitative measure of the properties of solids that control the acid strength. The integration of theory with kinetic data on well-defined catalysts can reveal how the structure and composition of solid acids, as well as the local reaction environment, control the elementary steps and the rates of acid-catalyzed reactions. More specifically, the tendency of a Brønsted acid site to act as a proton donor can be influenced by the catalyst composition, by the number and spatial location of other protons present, by interactions of the catalyst with a nominally inert support, by the presence of counter-balancing cations other than protons, and by interactions of neighboring sites on the catalyst with other basic molecules adsorbed as coreactants or products.

Keggin-type polyoxometalates (POMs) are ideal solids for studying the relationships between acid strength and catalytic rates and selectivities, because of their well-defined structure, synthetic accessibility, and useful properties as acid catalysts.[4−12] These POM solids have atomic configurations that are essentially unaffected by composition, thus allowing variations in acid strength without concomitant changes in structure that would render conclusions about composition effects equivocal. The catalytic rates and selectivities achieved on polyoxometalates vary with the identity of the central atom and with the replacement of some of the protons with other cations.[4−7,11−13] In addition, the full primary structure of the POM cluster can be rigorously described by ab initio methods.[8,9,14−16]

* Corresponding author. E-mail: mn4n@virginia.edu.
[†] Pennsylvania State University.
[‡] University of California at Berkeley.
[§] University of Virginia.

10.1021/jp8078748 CCC: $40.75
Published on Web 01/07/2009

We showed previously that the changes in 2-butanol dehydration rates that result from changes in the central atom reflect concomitant changes in the rate constant for kinetically relevant elimination steps and the equilibrium constants for the formation of inactive 2-butanol dimers.[7,13] A rigorous kinetic analysis confirmed that elimination occurs via E1 pathways and demonstrated the separate effects of the alcohol reactants and the central POM atom on the elimination rate constants and the dimer-formation equilibrium constants.[13] Elimination rate constants and dimer-formation equilibrium constants both increased as DFT-calculated deprotonation energies decreased and acid strength concurrently increased. The deprotonation energy (DPE) provides a useful probe of POM acid properties, because it accounts for the ability to form and separate the anionic POM cluster from the proton. We have also shown that the effects of higher DPE values on elimination barriers are compensated in part by the stronger electrostatic stabilization provided by the stronger conjugate base that forms upon deprotonation of such weaker acids.[13]

Herein, we report the results from density functional theoretical calculations together with previously reported rate data[13] to relate POM composition and its effect on deprotonation and stabilization energies to the rate and equilibrium constants relevant for dehydration catalysis. This study extends our previous communication[7] by carrying out a systematic theoretical analysis of acid-catalyzed alcohol dehydration for a broad range of catalysts and adsorbates that affect the relevant kinetic parameters. We describe in detail the proposed mechanisms and evaluate the impact of POM cluster composition; competing reaction pathways; specific alcohol reactants; coadsorption of alcohol reactants, water product molecules, and other n-donor molecules; support interactions; and the structural and reductive stability of the catalyst on the performance of POM acid catalysts for the dehydration of a series of alcohols including 2-butanol, 1-propanol, and 2-methyl-2-propanol. These factors influence the electronic properties of the POM cluster, which can ultimately influence catalytic rates.[4,6,7,10−13,17] Correlations between calculated deprotonation energies and measured dehydration activation barriers are shown here to reflect the ability of the POM to stabilize the anionic charge on the POM cluster. The ion-pair interaction energies also change with deprotonation energies[18] because they involve the formation and separation of R^+ (H^+ for DPE) and the POM anion. DPE differences among POM clusters are partially compensated by the concomitant stabilization of the ion pair that forms. The deprotonation energy and the stabilization energy of the ion pair arise from elementary steps that are quite different from one another. The former requires a complete separation of the H^+ and POM anion upon deprotonation, whereas the latter involves only a partial separation of the R^+ and the POM anion that stabilizes the ensuing ion pair.

2. Computational Methods

All of the computational results reported herein were obtained using ab initio density functional theory (DFT) calculations as implemented in the total-energy and molecular dynamics Vienna ab Initio Simulation Program (VASP).[19−21] Ultrasoft pseudopotentials were used to describe electron−ion interactions[22] with a plane-wave basis set cutoff energy of 400 eV. The Perdew−Wang (PW91)[23] form of the generalized gradient approximation was used to calculate exchange and correlation energies. The molecular system was represented within a $20 \times 20 \times 20$ Å^3 cubic unit cell, where Brillouin zone sampling was restricted to the Γ point. Full geometry relaxation was performed for all equilibrium structures until the forces on all atoms were less than 0.05 eV Å^{-1}. The calculated bond distances and bond angles of primary Keggin structures agreed well with reported X-ray crystallographic data for the hydrated body-centered-cubic (bcc) structure of $H_3PW_{12}O_{40}\cdot 6H_2O$.[9,24]

The climbing image nudged elastic band (CI-NEB) method of Henkelman and Jonsson[25−27] was used to isolate transition states. A series of images connecting the initial and final states were optimized along the direction perpendicular to the normal vector between neighboring images. The transition state was identified as the image with the highest energy along the path between reactants and products with a tangent force that is less than 0.05 eV Å^{-1} and atomic forces that are less than 0.05 eV Å^{-1}. A number of the transition states were confirmed by subsequently carrying out frequency calculations to establish the single imaginary vibrational frequency along the reaction coordinate. Zero-point vibrational energies (ZPVEs) were not routinely calculated because of the computational demands associated with developing a Hessian matrix for the entire POM−adsorbate system, as well as the inaccuracies inherent in harmonic oscillator treatments of low-energy vibrations in hydrocarbon fragments which weakly interact with POM surfaces. The low-energy (and low-frequency) vibrations should not significantly affect the ZPVE; however, the anharmonicity of these modes,[28] as well as the convergence specified in the constrained numerical Hessian,[8,29] make rigorous calculation of ZPVE corrections computationally intractable. An estimated ZPVE correction is presented in a later section for the water elimination activation barrier over $H_3PW_{12}O_{40}$, and corrections over other compositions are expected to be similar. The changes in the activation and dimer formation energies due to changes in the POM composition or changes in the reaction environment would therefore be unaffected by the lack of ZPVE corrections, but absolute values might differ from experimental barriers or adsorption energies. A Bader charge analysis[30−32] was used to assign electron density to specific atoms in order to estimate formal charges and establish the charge associated with specific fragments for an adsorbed state. In the Bader approach, the charge density between atoms is split between two atoms along a dividing plane known as the zero-flux surface. The surface lies perpendicular to the atoms at the point between the two atoms where the charge density reaches a minimum.

The adsorption energies were defined as the difference in energy between the adsorbed intermediate and the POM cluster ($E_{\text{adsorbate+POM}}$) and the separated adsorbate ($E_{\text{adsorbate}}$) and POM cluster (E_{POM})

$$\Delta E_{\text{ads}} = E_{\text{adsorbate+POM}} - E_{\text{adsorbate}} - E_{\text{POM}} \quad (1)$$

When coadsorption was considered, the energy of the POM cluster with the coadsorbed species was used as the reference instead of that of the POM cluster alone. Each activation barrier (E_{act}) was calculated as the difference in energy between the transition state and the preceding intermediate (unimolecular reaction) or the preceding intermediate and the gas-phase reactant (bimolecular reaction).

The deprotonation energies (DPEs)[33] were calculated as the energy required to separate the proton and conjugate-base species (A^-) to an infinite distance

$$\text{DPE} = E_{H^+} + E_{A^-} - E_{AH} \quad (2)$$

The calculations for charged states were carried out by applying an equal but opposite, homogeneous background charge to the cell. The energies were subsequently corrected to account for the resulting monopole, dipole, and quadrupole interactions

SCHEME 1: Elementary Steps in the Proposed E1 and E2 Mechanisms for Alcohol Dehydration over the Keggin-Type Polyoxometalates[a]

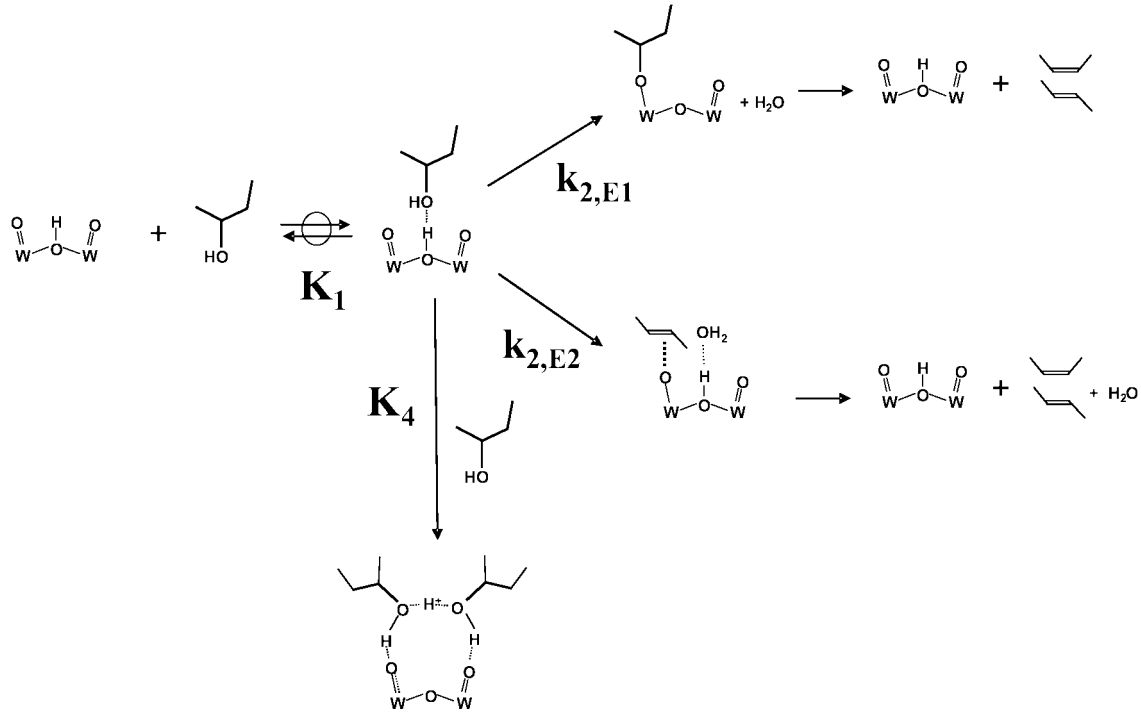

[a] $k_{2,E1}$ and $k_{2,E2}$ refer to the elementary elimination step rate constants for the E1 and E2 paths, respectively. K_1 and K_4 refer to the adsorption constant for the alcohol monomer and the equilibrium constant for dimer formation, respectively.

using the approach developed by Makov and Payne,[34] which involves calculating the energy difference between the actual periodic system and the same monopole/dipole/quadrupole complex in vacuum.

The composition of POM is abbreviated throughout as HXM, where X is the central atom and M is the addenda atom. The POM cluster contains central (O_a), terminal (O_d), edge-sharing (O_c), and corner-sharing (O_b) oxygen atoms. The latter three act as possible proton binding sites, whereas the central oxygen atoms, which are inaccessible, do not. Although edge-sharing oxygen (O_c) atoms were found to be the preferred proton location sites on HPW, they differ in energy by less than 10 kJ mol^{-1} from the other possible sites.[9] For consistency in comparing different POM compositions, we considered protons only at the O_c site when calculating DPEs and also assumed these to be the adsorption and reaction site for 2-butanol reactants.

The relative energies for 2-butanol dehydration and deprotonation depend on the specific locations of the protons not directly involved in the reaction. The proton positions were therefore held constant in order to decouple their influence on the kinetics from that of other factors. A specific example of the impact of proton position on dehydration energetics is provided in the Results and Discussion section. We assumed that protons are distributed similarly among the different oxygen atoms (O_b, O_c, and O_d) in POM clusters of different composition. We therefore used the lowest-energy proton positions found here to evaluate the relative energetics for other systems. The locations of the first three protons are those determined as optimal for HPW and reflect the specific O_c, O_b, and O_c sites reported earlier by Janik et al.[9] The fourth proton prefers to bind to an O_d atom, as shown for HSiW,[35] whereas the fifth proton preferentially binds to an O_b atom, as shown for HAlW.[35] In all cases, the reported DPE and 2-butanol adsorption energies consider only the proton bound to the edge-sharing oxygen atom (O_c) in the POM cluster. The alcohol dehydration reaction was assumed to occur within the plane defined by the O_d—W—O_c atoms, previously shown to be preferred for carbenium-ion transition states in olefin adsorption and alkylation on HPW.[8]

3. Results and Discussion

3.1. Alcohol Dehydration Pathways and Kinetics. We have shown that the rates of alcohol dehydration on SiO_2-supported POM clusters depend on the rate constant for the elimination elementary step (k_2) and the equilibrium constant for the formation of unreactive alcohol dimers (K_4) (see Scheme 1).[7,13] The reaction proceeds via the quasi-equilibrated adsorption of the alcohol on POM Brønsted acid sites to form adsorbed species that subsequently eliminate water via an E1 or E2 elimination pathway.[36−39]

The initial steps in the E1 and E2 paths are sketched in Scheme 1. In both cases, the alcohol molecule initially adsorbs by forming a hydrogen bond between the proton on the POM and the alcohol oxygen atom. The E1 path proceeds via the protonation of the adsorbed alcohol and the subsequent heterolytic cleavage of the C—O bond, resulting in the formation of an alkoxide intermediate and coadsorbed water. The dehydration is then completed by desorption of water and deprotonation of the alkoxide. The E2 mechanism is characterized by the concerted scission of C—O and C—H bonds in the alcohol, thus requiring direct interactions with an acidic proton and a neighboring basic oxygen atom in the POM. Both olefin and water are formed in a concerted step that regenerates the acid site by transferring the proton back to the basic POM oxygen atom. The dehydration reaction is then completed by subsequent desorption of olefin and water products and the proton transfer step that returns the proton to the original site.

The calculated equilibrium and transition states for 2-butanol adsorption and dehydration on HPW for both E1 and E2

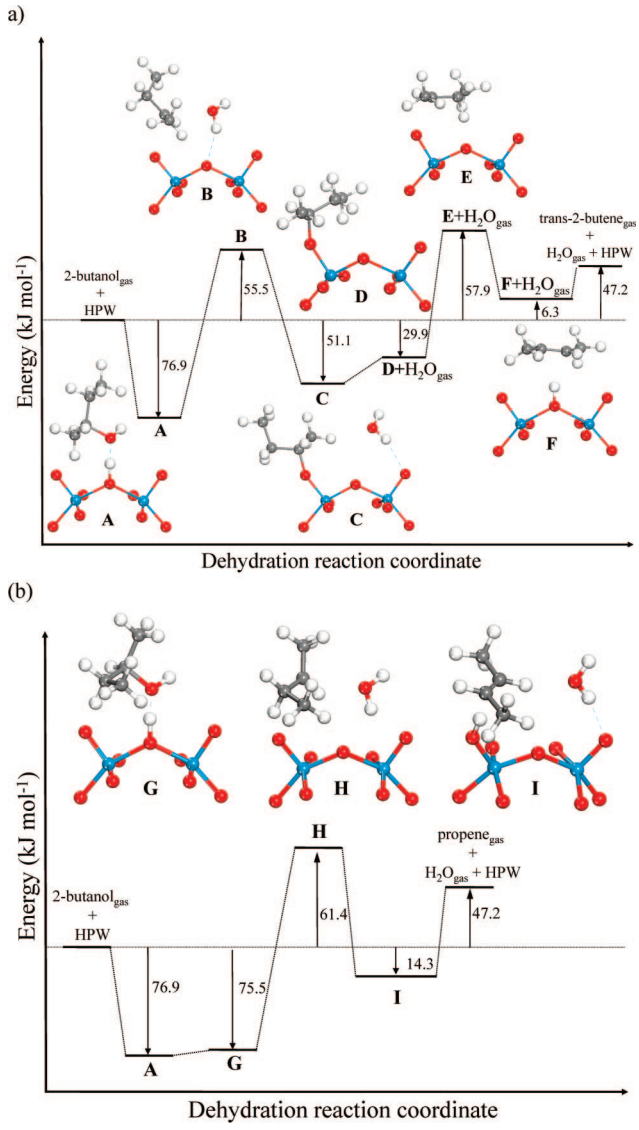

Figure 1. Reaction energy diagrams for 2-butanol dehydration via (a) the E1 mechanism and (b) the proposed E2 mechanism. All calculations were performed on the entire Keggin unit. Structures **B** and **H** are illustrated in Figure 2, and interatomic distances are given in Table 1.

pathways are depicted in Figure 1. The interatomic distances for the structures associated with each mechanism are given in Table 1. Alcohol adsorption onto the POM occurs via the formation of an $O_{alcohol}\cdots H^{+}—O_{POM}$ hydrogen bond (state **A**). The adsorption energy is −77 kJ mol^{-1}. In the E1 mechanism (Figure 1a), the products from the elimination step are a *sec*-butyl alkoxide and an adsorbed water molecule (state **C**). The alkoxide preferentially resides at a terminal (O_d) atom.[40] The reaction energy for water elimination from the adsorbed alcohol (state **A**) to form the bound alkoxy intermediate (state **C**) is +26 kJ mol^{-1}. The transition state for the E1 elimination path (state **B**) resembles a carbenium ion in that the substituents of the C_α atom are in the same plane, indicative of sp^2 hybridization. A Bader charge analysis confirmed the cationic character of the transition state, in which the total atomic charge on the hydrocarbon fragment in **B** is +0.85, whereas those in the Keggin unit and the water molecule are −0.88 and +0.03, respectively. The corresponding activation barrier for the elimination step in the E1 path is 132 kJ mol^{-1}. The transition state is illustrated in more detail in Figure 2a with all of the atomic labels provided. The $C_\alpha—O_{alc}$ and $C_\alpha—O_d$ bond lengths in the transition state are 2.64 and 3.18 Å, respectively, which are much larger than for typical covalent C—O bonds (∼1.5 Å). Thus, the alcohol C—O bond is fully broken but the O—C bond between the alkoxide intermediate and the Keggin structure is not yet formed at the transition state.

The subsequent desorption of water (state **D**) is endothermic (+21 kJ mol^{-1}). Olefin desorption occurs via a sequential process that involves the activation of the C—O bond to form a carbenium ion (**E**), similar in structure to that present at the dehydration transition state, and the subsequent proton transfer to form the physisorbed π-bound olefin, which then desorbs from the surface.[8,29,40] The olefin desorption step is simply the microscopic reverse of olefin protonation to form the corresponding alkoxide. We have previously reported olefin adsorption energies on different Keggin clusters.[8,29,40] The alcohol elimination and olefin desorption steps occur over the same O_d and O_c sites on the POM surface, but the carbenium-ion transition states in **B** and **E** differ in their orientation with respect to such surfaces. State **E** is slightly higher in energy than **B** in Figure 1a; however, the choice of requiring water desorption before olefin desorption is arbitrary. If water remained bound to the POM surface during olefin desorption, state **B** would be higher in energy than state **E**. The positive charge in state **B** is located farther from the anionic surface, because of the steric requirements of the elimination step in generating both the carbenium ion and the water species.

Although the elimination and alkoxide deprotonation steps have transition states that are at similar energies along the potential energy surface, the experimental comparison of 1-butene isomerization and alcohol elimination rate constants, with proper accounting for saturation coverage of butoxide or adsorbed butanol monomers, established the kinetic relevance of the elimination step, consistent with the DFT estimates of the E1 elimination barrier (132 kJ mol^{-1}) and the alkoxide deprotonation barrier (88 kJ mol^{-1}).[13] The elimination activation barrier will therefore be used throughout this study, together with dimer formation equilibrium, constants as an indication of relative rates of alcohol dehydration over various POM compositions.

The E2 elimination mechanism (Figure 1b) requires a slightly endothermic reorientation of the adsorbed alcohol (state **G**) to direct one of the hydrogen atoms on the C_β site toward the terminal oxygen so as to enable concerted C—O and C—H bond activation. This reorientation is equivalent to the pre-transition-state steps discussed for methanol dehydration pathways on zeolites.[41] The isolated transition state found via the CI-NEB method, which is shown in state **H** in Figure 1 (expanded in Figure 2b), resembles that found for the E1 path. It has strong carbenium-ion character, as indicated by sp^2 hybridization at the C_α atom and by a total Bader charge on the hydrocarbon fragment of +0.93. Whereas the $C_\alpha—O_{alc}$ bond (2.74 Å) is clearly broken in the transition state, the $C_{\beta 2}—H_{\beta 2}$ bond appears to remain intact. The $C_{\beta 2}—H_{\beta 2}$ distance (1.11 Å) in the carbenium ion is essentially identical to that in the adsorbed alcohol (1.10 Å). There is only a very weak interaction between the $C—H_{\beta 2}$ hydrogen and the terminal oxygen atom (O_d) on the Keggin unit in the transition state. This is evident from the long $H_{\beta 2}—O_d$ distance (2.13 Å) in the transition state, which is consistent with weak hydrogen bonding instead of covalent O—H bonds. In addition, the $W—O_d$ bond distance remains similar to that in the unperturbed POM and typical of tungstenyl (W═O) species. We therefore conclude that the $H_{\beta 2}$ proton is not perturbed at the transition state. Even though the CI-NEB

TABLE 1: Interatomic Distances (Å) within the Equilibrium and Transition-State Structures for the Conversion of Adsorbed 2-Butanol to Adsorbed *sec*-Butyl and Water Species[a]

E1 Mechanism							
structure	O_c—H	O_{alc}—H_{POM}	O_{alc}—C_α	C_α—$C_{\beta1}$	C_α—$C_{\beta2}$	C_α—O_d	W—O_d
A	1.08	1.40	1.49	1.51	1.52	3.18	1.71
B	2.11	0.98	2.64	1.45	1.46	2.42	1.75
C	3.06	0.98	4.27	1.51	1.52	1.47	1.80

Proposed E2 Mechanism								
structure	O_c—H	O_{alc}—H_{POM}	O_{alc}—C_α	C_α—$C_{\beta1}$	C_α—$C_{\beta2}$	W—O_d	$C_{\beta2}$—$H_{\beta2}$	$H_{\beta2}$—O_d
G	1.09	1.37	1.49	1.52	1.52	1.71	1.10	2.39
H	2.35	0.98	2.74	1.44	1.43	1.73	1.11	2.13
I	3.07	0.98	3.28	1.49	1.35	1.81	1.98	1.04

[a] Structures are illustrated in Figures 1 and 2, and atom labels are given in Figure 2.

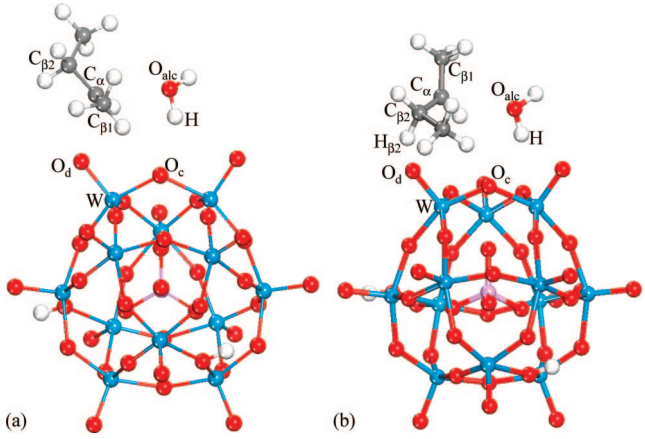

Figure 2. Transition states for the dehydration of 2-butanol to (a) a *sec*-butyl alkoxide and an adsorbed water molecule (structure **B** of Figure 1) and (b) a π-bound *trans*-2-butene and an adsorbed water molecule (structure **H** of Figure 1). Interatomic distances are given in Table 1.

approach should have been able to follow the simultaneous elimination and deprotonation steps, the isolated transition state did not differ from that in the nonconcerted E1 path. The CI-NEB approach seeks the highest-energy state along the minimum-energy path, which indicates that a "true" concerted E2 path is unlikely to occur. Subsequent attempts to isolate a concerted E2 transition state via constrained optimizations, in which the C—H bond was forced to break together with the C—O bond, also failed to find a saddle point. We cannot exclude the existence of a saddle point corresponding to a concerted pathway on the potential energy surface, but we conclude that one is unlikely to exist at energy levels similar to those available for nonconcerted E1 routes. The activation of the C—H bond by a basic O atom on HPW does not occur simultaneously with C—O bond activation. C—H activation occurs only after the C—O bond is broken and the carbenium ion is formed. This is consistent with measured kinetic isotope effects near unity for deuterium-labeled 2-propanol, which indicate that the C—H bond is not significantly involved in the elimination transition state.[13]

The isolated transition state (state **H**) for our CI-NEB analysis of the putative E2 path shown in Figure 1b is nearly identical to that for E1 elimination (state **B**) They differ only in that the C—$H_{\beta2}$ bond is better positioned for subsequent C—H activation by the O_d atom along this path. This places the new transition state (**H**) slightly farther from the Keggin surface than in the E1 route, causing a slight increase in energy. The barrier for this second path (138 kJ mol^{-1}) is thus slightly higher than for the initial E1 mechanism (132 kJ mol^{-1}). This path avoids the intervening formation of a stable alkoxide intermediate but instead goes on to activate the C—H bond.

The two different transition states found here can simply be viewed as two different configurations for the E1 path that can be statistically sampled, as they exist along a relatively flat potential energy surface near the transition state. Small entropic changes determine the final state (alkoxide or π-bound alkene) into which the molecule will ultimately fall. The relative contribution of the two pathways is thus determined by the energies and partition functions of the respective transition states for the two paths. The computational results clearly show that the E1 mechanism is the dominant path. The calculated transition state agrees very well with experimental results from kinetic isotope studies, which indicate that the transition state has significant carbenium-ion character and a large pre-exponential factor due to the significant gain in entropy of the transition state.[13]

The adsorbed butanol monomer can also interact with another alcohol molecule (as depicted in Scheme 1) or with a water molecule to form more stable protonated oligomers. Dimers are unreactive and occupy sites otherwise accessible for reactive monomers and thus decrease alcohol dehydration rates.[7,13] Rate data are consistent with the conclusion that adsorption equilibrium constants for butanol monomers and dimers are much greater than for water monomers and dimers and that those for alcohol—water mixed dimers are similar to those for alcohol dimers.[13] The concentration of the latter, however, can be neglected at the low H_2O concentrations prevalent in experiments at low alcohol conversions. The rate expression for 2-butanol dehydration is then given by[13]

$$r = \frac{k_2[H^+]}{1 + K_4[C_4H_9OH]} \tag{3}$$

where k_2 is the rate constant for E1 elimination and K_4 is the equilibrium constant for butanol dimer formation. This equation accurately describes all experimental data for 2-butanol and for alcohols and ethers on all POM catalysts tested (HPW, HSiW, HSW, HAlW, HCoW, HPMo).

Next, we examine how changes in the identity of the alcohol and in the POM composition influence the energies of the relevant transition state and of the reactive and unreactive adsorbed species. We estimate the energy differences between elimination transition states and adsorbed monomers, $E_{act}^{(2)}$, which represent the activation barrier for the k_2 rate constant, as well as the formation energies for dimer species, $\Delta E_{ads}^{(2)}$,

TABLE 2: Adsorption Energies (kJ mol^{-1}) and Activation Barriers (kJ mol^{-1}) for E1 Mechanism for Primary, Secondary, And Tertiary Alcohol Dehydration over HPW

		E1 mechanism	
alcohol	ΔE_{ads}	ΔE_{dehy}	E_{act}
1-propanol	−74	31	139
2-butanol	−77	26	132
2-methyl-2-propanol	−70	24	85

which control the dimer equilibrium constant, K_4. These properties are specifically examined as a function of the POM deprotonation energy, varied through changes in the identity of the POM central and addenda atoms.

3.2. Effects of Alcohol Structure on the Elimination Kinetics. The structure of the alcohol can strongly influence the stability of the carbenium ion and, in turn, affect both the rate and adsorption constants involved in the formation of carbenium-ion transition states or intermediates. In the absence of steric effects, the more stable carbenium ions would lead to higher rates because they result in transition states with lower activation barriers. These effects were explored in this work by varying the degree of substitution at the C_α atom in the alcohol and calculating the resulting elimination activation barriers. The DFT-calculated E1 barriers on HPW are listed in Table 2 for 1-propanol, 2-butanol, and 2-methyl-2-propanol.[29] The barriers for carbenium-ion formation decrease as the number of carbon substituents bound to the C_α atom increase. This trend reflects an increased stability in the elimination transition states as a result of the greater ability of the more substituted organic species to accommodate the required positive charge. The carbenium-ion stability decreases in the order tertiary > secondary > primary. Experimentally, a linear correlation of the elimination activation barriers with carbenium-ion stability, defined here as the enthalpy differences of the carbenium ion and the H_2O molecule with respect to the proton and the alcohol reactant, was also observed, consistent with the late elimination transition-state structure calculated and the effects of alcohol identity on the elimination barriers discussed above.[13] The experimental primary/secondary elimination barrier difference (20 kJ mol^{-1}) is greater than the DFT-calculated barrier difference of 7 kJ mol^{-1}. This might be a consequence of the single reaction trajectory considered, as the primary carbenium ion locates substantially closer to the anionic surface than the secondary carbenium ion, a result that might be unique to the path considered. The relatively small difference in barrier between primary and secondary eliminations is consistent with the calculated barrier for ethylene adsorption, which is also lower than expected based on relative carbenium-ion stability.[40]

3.3. Thermodynamics of Dimer Formation. n-Donor species, such as the alkanol reactants or the water products, inhibit dehydration rates by the formation of unreactive and stable dimers.[7,13,17,42] These effects are accurately described by a rate equation (eq 3) in which dimers account for the observed inhibition.[7] The preferred structure for the adsorbed 2-butanol dimers on an isolated HPW cluster is shown in Figure 3. The proton is fully abstracted from the POM, and an $O_{alc}—H^+—O_{alc}$ bridge is formed between two butanol molecules. A local network of hydrogen bonds forms between the OH groups on the alcohols and the terminal O_d atom in the POM structure. The energy for adsorption of a 2-butanol molecule on a POM Brønsted acid site is estimated as −77 kJ mol^{-1}, and the adsorption of the second 2-butanol is even more exothermic (−84 kJ mol^{-1}).

Water is formed in dehydration reactions, and its dimers ($H_5O_2^+$) or mixed 2-butanol/water dimers might also form at sufficiently high conversions and H_2O pressures. The adsorption energies for these species are reported in Table 3, where the two 2-butanol/water species listed are identical except for the (thermodynamically inconsequential) order of adsorption. The adsorption of 2-butanol on the POM and on either adsorbed water or adsorbed butanol is stronger than the adsorption of water on either of these surface species.

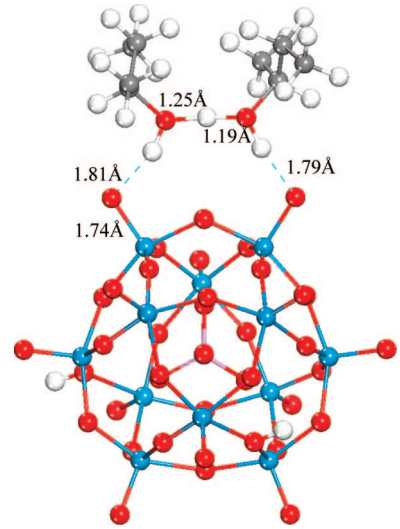

Figure 3. Two 2-butanol molecules interacting with the HPW Keggin unit through formation of a protonated dimer, $(C_4H_{10}O)_2H^+$. Hydrogen bonds between the alcohol groups and terminal oxygen atoms of the Keggin unit are formed.

TABLE 3: Adsorption Energies of 2-Butanol, Mixed 2-Butanol−Water, and Water Dimer Species[a]

first adsorbate, second adsorbate	$\Delta E_{ads}^{(1)}$ (kJ mol^{-1})	$\Delta E_{ads}^{(2)}$ (kJ mol^{-1})
2-butanol, 2-butanol	−77	−84
2-butanol, water	−77	−80
water, 2-butanol	−68	−89
water, water	−68	−69

[a] 2-Butanol dimer structure illustrated in Figure 3.

The elimination reactions of adsorbed dimers via E1 routes were also examined. This reaction occurs via scission of the C—O bond to convert one of the butanols to a butoxide bound to an O_d atom. The water molecule and the second 2-butanol molecule remain in a structure similar to that in the mixed dimer, with 2-butanol interacting through a hydrogen bond with a second O_d atom and the water molecule forming a hydrogen bond with the alcohol, as shown in Figure 4. The dehydration activation barrier for E1 elimination from the dimer was 175 kJ mol^{-1} (vs 132 kJ mol^{-1} for the butanol monomer), consistent with the unreactive nature of dimers implicit in the kinetic derivation leading to eq 3. These trends reflect the fact that the reactant structure is better stabilized by dimer formation than the transition state; thus, the energy of the reactant state is lowered further than that of the transition state, resulting in an increase in the activation barrier by 43 kJ mol^{-1}. We were unable to isolate an E2 path for the 2-butanol monomer; thus, we assumed that E2 paths would also be unlikely to occur with accessible barriers for the much more stable dimers.

3.4. Effect of POM Composition on Activation Barriers for Alcohol Dehydration and on Dimer Formation Energies. The identities of both the POM central atom and the addenda atom influence the stability of the charged species in the ion pair that forms at either the transition state or the butanol dimer.

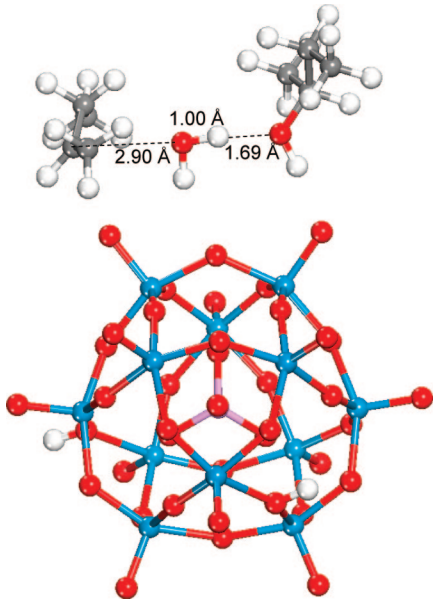

Figure 4. DFT-calculated transition state for the dehydration of 2-butanol from the 2-butanol dimer adsorbed to $H_3PW_{12}O_{40}$.

TABLE 4: 2-Butanol Adsorption and Dehydration Energies (kJ mol^{-1}) for Different Central Atoms of POM Clusters with Tungsten Addenda Atoms

		ΔE_{ads}			dehydration	
central atom	DPE	2-butanol	dimer	dehydration product[a]	$\Delta E_{reaction}$	$E_{act}^{(2)}$
Al	1121	−73	−70	−101	20	146
Si	1105	−76	−77	−99	24	140
P	1087	−77	−84	−98	26	132
S	1067	−80	−88	−96	32	127
max−min	54.2	7	18	4	11	19

[a] The adsorption energy of the dehydration product is the adsorption energy of *trans*-2-butene and water to form the alkoxide and water adsorbed state (structure **C** in Figure 1a).

A rigorous comparison of the intrinsic reactivity of protons in POM clusters requires that we normalize rates per proton, as changes in the composition can change the number of protons. In the experimental results to which we compare our simulations, all rate data have been rigorously normalized by the number of accessible protons measured during catalysis, and measured turnover rates have been interpreted in terms of rate and equilibrium constants for elementary steps, thus allowing direct comparisons with theory.

DFT-calculated activation barriers for the E1 elimination of adsorbed 2-butanol were determined for POM species with different central and addenda atoms (Table 4). Figure 5 compares these activation barriers and dimer formation energies, relative to the adsorbed alcohol, with those measured for the same step experimentally. The calculated and measured barriers show similar trends and are similar in value (to within the 20 kJ mol^{-1} accuracy of density functional theory[41,43,44]). DFT systematically overpredicts the activation barriers here by between 10−27 kJ mol^{-1}. This systematic overprediction reflects, in part, the lack of corrections for zero-point vibrational energy. ZPVE corrections were calculated to lower the activation barrier for E1 elimination by 8.5 kJ mol^{-1} over HPW, with the approximation that only modes involving the adsorbate are altered. Additional inaccuracies caused by the periodic representation of separate charged states or by the accuracy of the exchange-correlation functional used are likely to account for

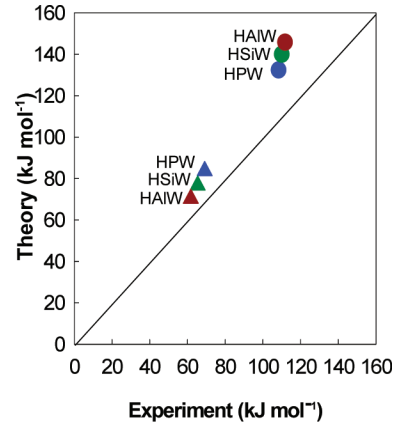

Figure 5. Comparison of the DFT-calculated barriers (●) and negative dimer formation energies (▲) for 2-butanol dehydration over $H_{8-n}X^{n+}W_{12}O_{40}$ structures with changes in the central atom.

the remaining systematic differences between theory and experiments.

Deprotonation energy estimates provide a measure of acid strength that we correlate here with activation barriers. The activation barrier for the elimination step ($E_{act}^{(2)}$) increases in parallel with DPE [HSW (S^{6+}) < HPW (P^{5+}) < HSiW (Si^{4+}) < HAlW (Al^{3+})], where the HSW POM is expected to be the most active POM but has not been synthesized, so that its acid properties and reactivity are unknown.[35] A decrease in the valence state of the central atom results in an increase in the number of charge-balancing protons on the POM and thus an increase in its anionic charge. This increase in charge leads to an increase in both the deprotonation energies and the elimination barriers. The intrinsic activation barriers reported in Table 4 are relative to the adsorbed reactant state and are therefore directly comparable to those measured from the temperature dependence of the elimination rate constant. The adsorption energy for the alkoxide product that forms (ΔE_{ads} for the dehydration product) becomes slightly stronger with increasing DPE. Consequently, the dehydration reaction energies ($\Delta E_{reaction}$) become less endothermic as DPE increases.

The energies gained by the formation of a 2-butanol dimer from a monomer are listed for various POM compositions in Table 4, together with measured values. DFT estimates and measurements agree well, but theory overestimates the exothermicity of dimer formation. The greater charge separations (and charges) in the dimers relative to the monomers leads to dimer energies that depend more sensitively on composition and DPE than monomer energies. The difference between the lowest and highest dimer formation energies reported in Table 4, for example, is 18 kJ mol^{-1}, whereas this difference is only 7 kJ mol^{-1} for monomer energies. The results indicate that both dimer species and elimination transition states become more stable with decreasing DPE. The decrease in DPE reflects a more stable anionic conjugate base that forms upon deprotonation. Therefore, both the elimination rate constant (k_2) and the dimer equilibrium constant (K_4) increase in parallel with decreasing DPE, giving rise to kinetic compensation effects, evident in the form of the rate equation (eq 3). The rate becomes predominantly controlled by the k_2/K_4 term as alcohol pressures increase. Experimental k_2/K_4 ratios increased in the order HPW < HSiW < HAlW as DPE increased (i.e., weaker acid), leading to higher overall rates measured for the weaker acids at high reactant pressures.[7,13] In addition to changes in the central atom, changes in the addenda atom can also play an important role, as discussed next.

3.5. Effects of Addenda Atoms: Reduction and Decomposition Effects for HPMo and Consequences for Alcohol

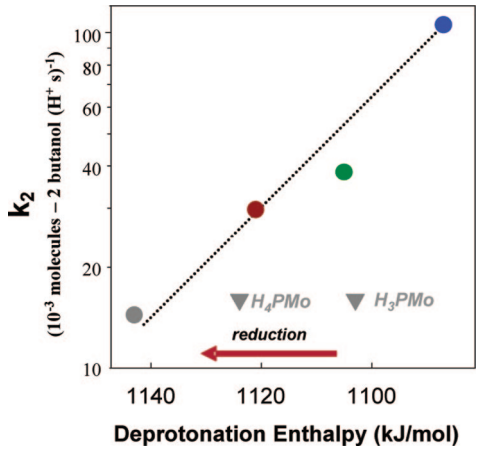

Figure 6. Comparison of the experimental rate constant for 2-butanol dehydration (k_2) and the DFT-calculated deprotonation energies of the $H_{8-n}X^{n+}W_{12}O_{40}$ and $H_3PMo_{12}O_{40}$ Keggin structures as a function of central atom and addenda atom. The reduced state of HPMo in the experiment is unknown, and therefore, the single experimental rate constant is plotted versus the calculated DPE with varying extent of reduction (see also Table 5).

Dehydration Catalysis. Reactivity comparisons must also account for any changes in POM composition caused by the possible reduction of the POM during pretreatment or reaction. At higher temperatures, the intact and/or reduced POM clusters can also undergo dehydration. Both reduction and dehydration become more important as Mo replaces W as the addenda atom in POM catalysts. 2-Butanol dehydration turnover rates (per H^+) were ~10 times lower on HPMo than on HPW.[45] The DFT-calculated activation barriers ($E_{act}^{(2)}$) are 141 and 132 kJ mol^{-1} for $H_3PMo_{12}O_{40}$ and $H_3PW_{12}O_{40}$, respectively, whereas the DPE values are higher for $H_3PMo_{12}O_{40}$ (1107 kJ mol^{-1}) than for $H_3PW_{12}O_{40}$ (1087 kJ mol^{-1}) The calculated activation barriers for 2-butanol elimination increase linearly with deprotonation energies, consistent with the logarithmic decrease in k_2 with DPE shown in Figure 6. The correlation of elimination rate constants (k_2) with calculated DPE values for POM clusters, however, does not appear to hold for $H_3PMo_{12}O_{40}$, as is shown in Figure 6. The discrepancy suggests the possible reduction of Mo centers in $H_3PMo_{12}O_{40}$ during reaction. This possibility was examined by adding an additional hydrogen atom to $H_3PMo_{12}O_{40}$ to form the partially reduced species $H_4PMo_{12}O_{40}$. The elimination activation barrier was found to increase from 141 to 149 kJ mol^{-1} upon reduction of $H_3PMo_{12}O_{40}$ to $H_4PMo_{12}O_{40}$, consistent with the increase in the deprotonation energy as $H_3PMo_{12}O_{40}$ (1107 kJ mol^{-1}) is reduced to $H_4PMo_{12}O_{40}$ (1124 kJ mol^{-1}). The reduction of $H_4PMo_{12}O_{40}$ to $H_5PMo_{12}O_{40}$ by the addition of a second H atom further increases both the DPE values (from 1124 kJ mol^{-1} for $H_4PMo_{12}O_{40}$ to 1145 kJ mol^{-1}) and the activation barriers (from 149 kJ mol^{-1} for $H_4PMo_{12}O_{40}$ to 154 kJ mol^{-1}).

If reduction is accompanied by protonation, which is the case for gas-phase reduction events, odd reduction states [e.g., $H_4PMo_{12}O_{40}$, with Mo(V)] are known to be unstable with respect to disproportionation according to the reaction $2H_4PMo_{12}O_{40} \leftrightarrow H_3PMo_{12}O_{40} + H_5PMo_{12}O_{40}$.[46] Even-numbered reduction events, on the other hand, are much more favorable than odd reductions as they result in the formation of stable molecules. Our calculated reduction energies are consistent with this observation, as the two-electron reduction of $H_3PMo_{12}O_{40}$ to $H_5PMo_{12}O_{40}$ (−161 kJ mol^{-1}, consisting of −57 kJ mol^{-1} for the first electron and −104 kJ mol^{-1} for the second electron) is 47 kJ mol^{-1} more favorable than two single-electron reductions to $2H_4PMo_{12}O_{40}$ (−114 kJ mol^{-1}). The stable $H_5PMo_{12}O_{40}$ structure is thus the more relevant reduction intermediate. The calculated DPE value for the more stable $H_5PMo_{12}O_{40}$ structure also moves the HPMo data point in Figure 6 much closer to the correlation line between k_2 and DPE.

TABLE 5: 2-Butanol Adsorption and Dehydration Energies (kJ mol^{-1}) for Various Forms of HPMo That Might Be Present in the Reaction Environment

		ΔE_{ads}		dehydration	
	DPE	2-butanol	dehydration product[b]	$\Delta E_{reaction}$	$E_{activation}$
$H_5PMo_{12}O_{40}$ (a)[a]	1125	−63	−75	40	149
$H_3PMo_{12}O_{39}$ (a)[a]	1109	−70	−71	41	147
$H_5PMo_{12}O_{40}$ (b)[a]	1145	−61	−67	41	154
$H_3PMo_{12}O_{39}$ (b)[a]	1128	−65	−74	39	147
$H_4PMo_{12}O_{40}$	1124	−60	−67	40	149
$H_2PMo_{12}O_{39}$	1109	−66	−69	44	146
$H_3PMo_{12}O_{40}$	1107	−64	−73	38	141
$HPMo_{12}O_{39}$	1098	−67	−75	39	139

[a] Two proton positions were explored for the addition of the fifth proton to $H_5PMo_{12}O_{40}$ and its derivative water-defect structure. Those designated with an "a" locate the additional proton on an O_b atom. Those designated with a "b" locate the additional proton on an O_d atom. The O_b atom location is more stable by 55 kJ mol^{-1} in the intact $H_5PMo_{12}O_{40}$ structure. [b] The adsorption energy of the dehydration product is the adsorption energy of *trans*-2-butene and water to form the alkoxide and water adsorbed state (structure **C** in Figure 1a).

Although structural decomposition of the HPW clusters was not evident during butanol dehydration studies, HPMo clusters appeared to reduce, as evidenced by changes in their color and UV−visible spectra.[45] Ohtsuka et al.[47] also detected color changes in HPMo, indicative of reduction, during catalytic dehydration of *tert*-butyl alcohol. Other studies have shown that HPMo structures can also undergo the loss of structural water via dehydration with concomitant loss of acidic protons. Thermogravimetric measurements by Bardin et al.[10] indicated the loss of structural water from HPMo Keggin clusters via removal of an oxygen atom and two acidic protons from Keggin units starting at ~423 K[10] and at even lower temperatures during longer treatments under anhydrous conditions.

We consider here the partial dehydration of HPMo clusters as the removal of two protons from $H_3PMo_{12}O_{40}$ and the O_b atom located farther from the remaining proton, because this was previously calculated to be the preferred site for initial decomposition.[35] The alcohol elimination barriers, monomer and dimer formation energies, and DPE values for the intact as well as the dehydrated forms of $H_3PMo_{12}O_{40}$ shown in eqs 4−6 are reported in Table 5.

$$H_3PMo_{12}O_{40} \rightarrow HPMo_{12}O_{39} + H_2O \quad (4)$$

$$H_4PMo_{12}O_{40} \rightarrow H_2PMo_{12}O_{39} + H_2O \quad (5)$$

$$H_5PMo_{12}O_{40} \rightarrow H_3PMo_{12}O_{39} + H_2O \quad (6)$$

The dehydration of $H_3PMo_{12}O_{40}$ to $HPMo_{12}O_{39}$ results in an increase in acid strength. The DPE value decreases from 1107 to 1098 kJ mol^{-1} and is accompanied by a slight decrease in the elimination activation barrier from 141 to 139 kJ mol^{-1}. The increase in acid strength, however, also slightly increases the 2-butanol adsorption strength by 2 kJ mol^{-1}. This likely leads to a very small increase in the 2-butanol dimer adsorption strength, which would slightly increase K_4. The reduction of the dehydrated $HPMo_{12}O_{39}$ to $H_2PMo_{12}O_{34}$ increases the value of DPE from 1098 to 1109 kJ mol^{-1} and the

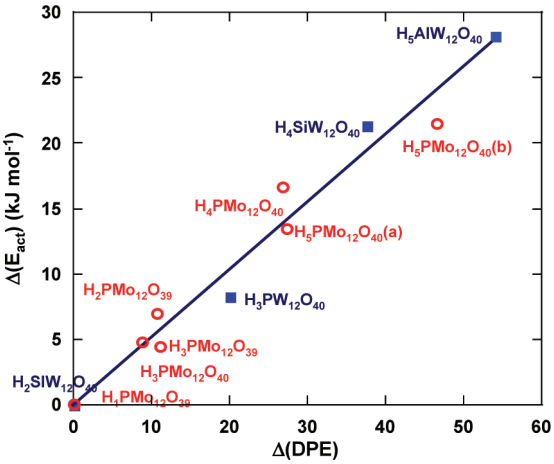

Figure 7. Effects of the reduction of the addenda atoms and the loss of structural water from the POM clusters on the elimination barriers. The comparison of the activation barrier for 2-butanol dehydration is plotted versus POM deprotonation energy as a function of the changes in HXW central atoms (○) and HPMo reduction (■).

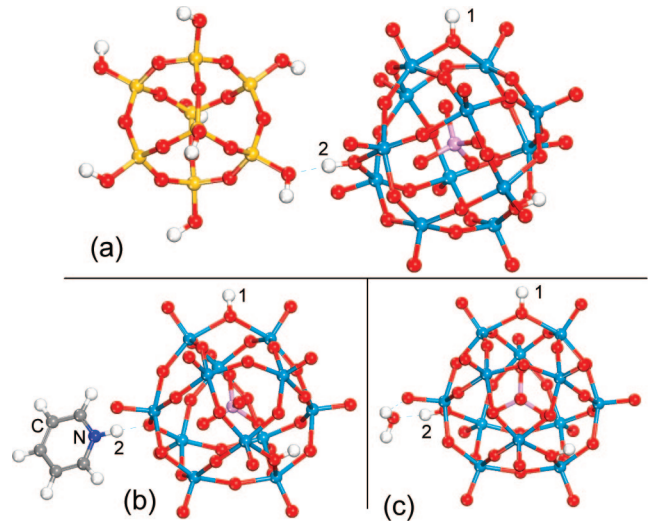

Figure 8. Structures of (a) $Si_8H_8O_{20}$, (b) pyridine, and (c) water bound to the HPW Keggin unit. In each case, adsorption is at a proton associated with an O_c atom labeled 2. 2-Butanol adsorption and dehydration was subsequently considered at proton site 1.

2-butanol elimination activation barriers from 139 to 146 kJ mol^{-1}. The subsequent reduction of $H_2PMo_{12}O_{39}$ to $H_3PMo_{12}O_{39}$ further increases the DPE to 1128 kJ mol^{-1} and the elimination barrier to 147 kJ mol^{-1}.

The changes that result in the reduction of the POM very closely follow the same correlation between the calculated elimination activation barrier and the calculated DPE established for the changes in the central atoms, as shown in Figure 7. In summary, any event that leads to a transfer of electrons or electron density into the POM (i.e., reduction) stabilizes the interaction of the conjugate base (the anionic POM cluster) and its affinity for the charge-balancing protons (i.e., DPE), resulting in a concomitant decrease in acid strength. We demonstrate in the next section that interactions of the POM with other adsorbates, with the support, and even with another POM cluster all result in similar transfers of electron density to the outer shell of the POM, thus increasing the POM's DPE and lowering its acidity.

3.6. Effects of Support Interactions, Coadsorbates, and Location of Protons. The actual environment around the supported POM clusters is more complex than that in the isolated clusters that we have considered in the calculations up to this point. Interactions with supports, vicinal POM clusters, or coadsorbates can influence the properties of acidic protons and their reactivities. Also, charge-compensating cations, coadsorbed species, and the precise location of the protons can introduce effects that would make comparisons between theory and experiment less accurate or faithful. In the following discussion, we examine the potential impact of each of these effects on the DPE and the kinetic parameters relevant to elimination reactions of alcohols.

The explicit and rigorous inclusion of an extended support is computationally prohibitive. We have chosen instead to simulate such interactions using a polyhedral oligomeric silsesquioxane (POSS) model structure with OH groups at each of its eight corner sites [$Si_8O_{12}(OH)_8$, Figure 8a] as a surrogate for the silica support. We consider the properties of the POM protons not associated with the POSS cluster. POSS clusters interact with HPW protons, forming $O_{POSS\text{-}OH}\cdots H_{POM}—O_c$ hydrogen bonds in an exothermic reaction (−60 kJ mol^{-1}) that renders such interacting POM protons unreactive in subsequent adsorption or protonation events. The DPE of a residual proton on the POM cluster increases from 1087 kJ mol^{-1} for the free HPW to 1103 kJ mol^{-1} for similar structures bound to POSS, indicating that the interaction between POM protons and POSS structures decreases the POM acid strength. The $O_{POSS\text{-}OH}\cdots H_{POM}—O_c$ H-bonding interactions lead to a larger residual negative charge on the oxygens of the POM cluster, because electron density is transferred from the model POSS support to the more electronegative POM cluster. This increase in electron density on the POM cluster leads to a stronger attractive Coulombic interaction between the anionic shell and the protons, which, in turn, increases the POM deprotonation energies. The 2-butanol dehydration barrier, $E_{act}^{(2)}$ (Table 6), increases concurrently upon interactions of HPW with POSS, as the transition state also becomes less stable because of the higher electron density in the POM cluster. This indicates that the interaction between the POM protons and the support would slightly increase dehydration activation barriers ($E_{act}^{(2)}$) over those on isolated POM clusters.

The opposite trend would be expected if a proton from a silanol group on the support formed a hydrogen bond with one of the oxygen atoms in the POM cluster, because the POM would then act as a proton acceptor. The charges on the POM, and specifically in its anionic shell, would therefore decrease, leading to consequent decreases in the deprotonation energy and the elimination activation barrier.

In addition to the POM−support interactions, high POM surface densities on support surfaces can lead to interactions among POM structures. In an effort to model these inter-POM hydrogen-bonding interactions and their effect on DPE, we calculated the energy required to remove a noninteracting proton from a $H_3PW_{12}O_{40}\cdots H_3PW_{12}O_{40}$ dimer via the following step

$$H_2PW_{12}O_{40}—H\cdots H_3PW_{12}O_{40} \rightarrow HPW_{12}O_{40}—H\cdots H_3PW_{12}O_{40}+H^+ \quad (7)$$

The protons on the proton-donating POM cluster have characteristically different deprotonation energies than those on the proton-accepting POM. The DPE values on the proton-donating POM increase from 1094 to 1126 kJ mol^{-1} as a result of the interaction of two POMs, whereas those on the proton-accepting POM decrease from 1094 to 1038 kJ mol^{-1}. This is due to the very different stabilization of the resulting anion that forms upon deprotonation. The deprotonation of a proton-donating POM

TABLE 6: 2-Butanol Adsorption and Dehydration Energies (kJ mol^{-1}) for Different Central Atoms of POM Clusters with Tungsten Addenda Atoms and Including Coadsorbates on a Second Proton, Movement of the Second Proton, and Substitution of Na and Cs Countercations

			ΔE_{ads}		dehydration	
central atom	coadsorbate	DPE	2-butanol	ΔE_{ads} dehy. prod.[a]	$\Delta E_{reaction}$	$E_{act}^{(2)}$
P	2,6-DTP (1)[b]	1096	−77	−95	30	138
P	2,6-DTP (2)[b]	1100	−76	−92	31	141
P	2,6-DTP (3)[b]	1175	−67	−80	34	156
P	2,6-DTP (4)[b]	1172	−67	−81	34	153
P	pyridine	1143	−71	−85	33	146
P	water	1090	−77	−95	29	137
P	2-butanol	1104	−75	−92	30	136
P	POSS[c]	1103	−80	−98	29	135
P	move H to O_d	1094	−75	−93	29	136
P	$NaH_2PW_{12}O_{40}$	1124	−72	−88	31	145
P	$CsH_2PW_{12}O_{40}$	1157	–	–	–	–
P	$CsH_2PMo_{12}O_{40}$	1177	–	–	–	–
Al	2,6-DTP[b]	1133	−75	−104	19	146
Al	pyridine	1169	−68	−89	27	155

[a] The adsorption energy of the dehydration product is the adsorption energy of *trans*-2-butene and water to the alkoxide and water adsorbed state (structure **C** in Figure 1a). [b] 2,6-DTP is 2,6-di-*tert*-butylpyridine. Different adsorbed configurations were considered, listed in order of increasing adsorption energy (increasing stability): (1) adsorbed with proton on an O_C atom and not transferred to 2,6-DTP, (2) similar but with tert-butyl groups rotated to minimize repulsive interactions with the Keggin unit, (3) proton transferred across the H bond to bind directly with the N atom of the substituted pyridine, and (4) protonated 2,6-DTP forms a N—H—O_d hydrogen bond. [c] POSS is an OH-substituted POSS cube—$(OH)_8Si_8O_{12}$—used to represent interaction of the Keggin unit with a silica support.

TABLE 7: Energies of Adsorption to HPW and HAlW and Changes in Deprotonation Energy (of Proton 1) Due to Adsorption (to Proton 2)

adsorbate	ΔE_{ads} (kJ mol^{-1})	ΔDPE (kJ mol^{-1})
HPW		
2,6-di-*tert*-butylpyridine (1)[a]	−24	10
2,6-di-*tert*-butylpyridine (2)[a]	−45	14
OH POSS $(OH)_8Si_8O_{12}$	−60	17
water	−67	4
2-butanol	−78	17
pyridine	−150	57
2,6-di-*tert*-butylpyridine (3)[a]	−155	88
2,6-di-*tert*-butylpyridine (4)[a]	−168	86
HAlW		
2,6-di-*tert*-butylpyridine (1)[a]	−24	11
pyridine	−139	48

[a] 2,6-di-*tert*-butylpyridine: adsorbate configurations as described in footnote of previous table.

bound to an identical proton-accepting POM cluster is less favorable than the deprotonation of the noninteracting POM cluster, because the resulting anion that forms on the proton-donating POM interacts repulsively with a terminal oxygen atom on the proton-accepting POM. In contrast, the deprotonation of the proton-accepting POM in the dimer is much more favorable than the deprotonation of the noninteracting POM. The anionic charge that forms upon deprotonation can be delocalized over both POM clusters, which stabilizes its formation over that for a noninteracting POM cluster. In the optimized POM dimer that forms upon deprotonation, the proton is equally shared between the oxygen atoms on the proton-donating and proton-accepting POM structures. This is shown in Scheme 2.

Under reaction conditions, the protons are likely mobile, and thus experiments measure the average energy from the ensemble of both the more acidic protons from the proton-accepting POMs and the less acidic protons from the proton-donating POM clusters. The average value might not change from that of the isolated POM, as the more acidic protons are balanced by the less acidic protons. In addition, the "shared proton" that bridges the two POM clusters is rather mobile[48] and might reposition itself to enhance stabilization of the anion. These trends are consistent with the experimental data, which show undetectable changes in k_2 and K_4 as the surface density of POM clusters on silica supports is increased. The lack of surface-density effects during 2-butanol dehydration reactions can also be attributed to the more favorable interaction of protons with 2-butanol reactants to form adsorbed 2-butanol monomers and dimers than the interaction of protons with another POM cluster.

Thus far, we have considered protons located at fixed positions on POM surfaces, because all calculations were performed at 0 K. In practice, protons are delocalized among different locations with small energy differences at relevant reaction temperatures, especially in the presence of water or alcohol, which facilitate proton mobility.[49] Transferring a proton from an O_c site to an O_d site slightly increases DPE values (from 1087 to 1094 kJ mol^{-1}) for a proton at a second O_c site away from the O_d site. The dehydration barrier at this O_c-bound proton increases slightly (Table 6) as a result of the change in the proximity of the protons at other binding sites. These small changes in deprotonation energy indicate that the consequences of fixing protons at specific locations on DPE are negligible (<2 kJ mol^{-1}).

Coadsorbed species can also influence the energy required to remove the residual free protons, as shown in the results given in Tables 6 and 7. The adsorption of 2-butanol, 2-butanol dimers, pyridine (Figure 8b), or water (Figure 8c) at OH sites on the POM cluster can indeed alter the deprotonation energies of the residual protons of the POM clusters and the elimination barriers. Table 6 reports DPE values and 2-butanol dehydration activation barriers for adsorbed 2-butanol when a single molecule of each of these species is preadsorbed onto the HPW cluster. The results reveal that the DPE values of the HPW cluster with different coadsorbates scale with the basicity of the coadsorbate. Strong bases, such as pyridine and 2,6-di-*tert*-butylpyridine (2,6-DTP), abstract the proton to form a pyridinium−anionic POM structure such as that shown in Figure 8b. The bulky nature of 2,6-DTP leads to differences in how strongly it adsorbs at different sites on the POM cluster. The

SCHEME 2: Interaction and Deprotonation of a Proton-Donating POM (D) and a Proton-Accepting POM (A) Dimer Complex[a]

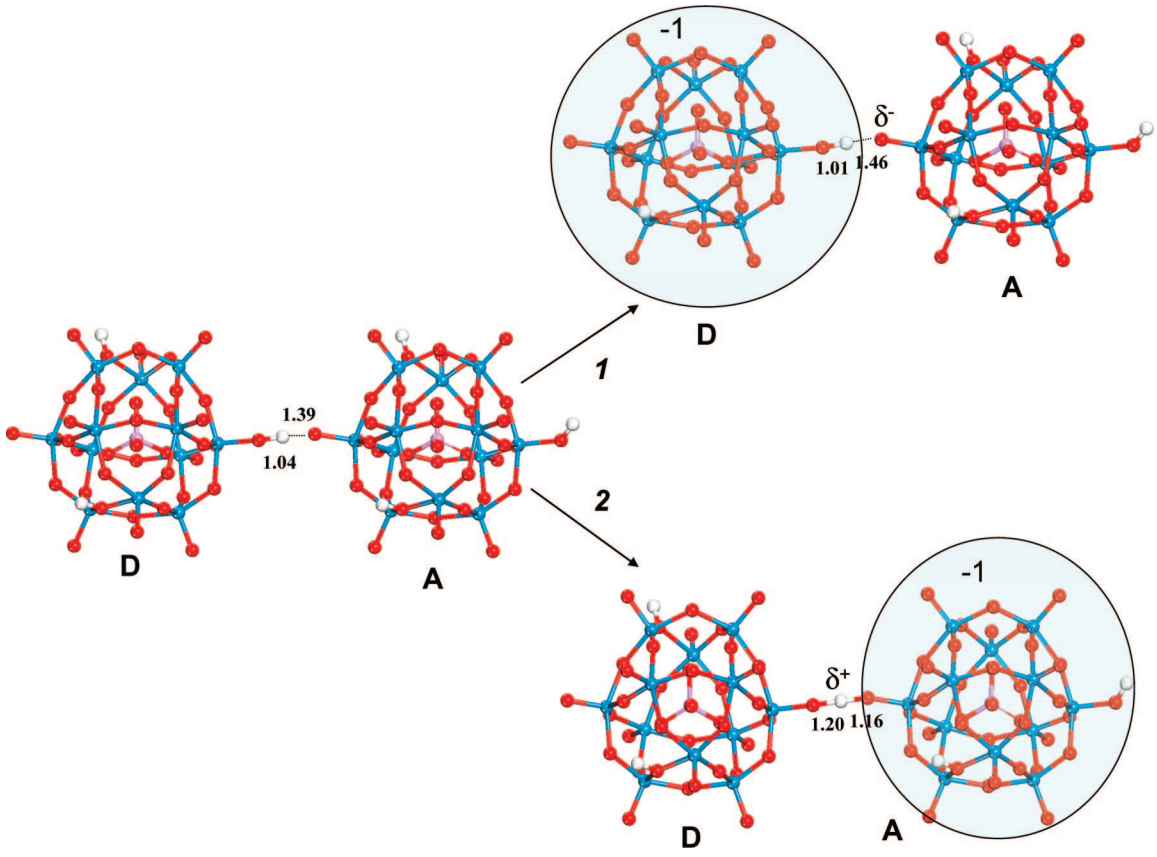

[a] Path 1 leads to a repulsive interaction between the POM(−1) anion on D and the δ^- charge density on the terminal oxygen of the proton-accepting POM (A). This results in a destabilization of the anion, which decreases the acidity of the POM dimer versus that for the isolated POM cluster. Path 2 results in a stabilizing interaction between the POM(−1) anion on A and the $\delta+$ charge density on the proton from POM D, where the anionic charge is delocalized over the entire dimer. This leads to an increase in the acidity of the dimer over that of the isolated POM molecule.

unhindered adsorption of 2,6-DTP at protons that reside on the terminal oxygen site is quite strong and results in the transfer of the proton from the POM to the 2,6-DTP to form a 2,6-di-*tert*-butylpyridinium ion. The adsorption of 2,6-DTP at a proton located at a bridging oxygen site, however, is hindered by repulsive interactions between the *tert*-butyl substituents and the neighboring tungstenyl (W═O) groups. This leads to a much weaker adsorption of 2,6-DTP onto the proton and precludes proton transfer. These two adsorption configurations (unprotonated and protonated 2,6-DTP) lead to different deprotonation energies for the other residual protons. The calculated DPE values of the residual protons increase in the order

$$\begin{aligned}&\text{HPW−water (1090 kJ mol}^{-1}\text{)} <\\ &\text{HPW−2,6-DTP (unprotonated) (1096−1100 kJ mol}^{-1}\text{)} \approx\\ &\text{HPW−2-butanol (1104 kJ mol}^{-1}\text{)} <\\ &\text{HPW−pyridine (protonated) (1143kJ mol}^{-1}\text{)} <\\ &\text{HPW−2,6-DTP (protonated) (1172−1175 kJ mol}^{-1}\text{)}\end{aligned} \quad (8)$$

In general, the more basic n-donors form stronger interactions with protons on Keggin structures. These interactions involve a charge transfer from the donor to the anionic shell of the more electronegative POM cluster and destabilize the anionic cluster that forms upon proton removal, thus making the residual protons less acidic. This slightly weakens the adsorption strength of 2-butanol on these substituted POM clusters from those on bare POM clusters (−77 kJ mol^{-1}). The 2-butanol adsorption strength decreases as the DPE of the n-donor POM complex increases.

The calculated E1 activation barriers for 2-butanol dehydration on POM clusters with coadsorbed n-donors (butanol, water, 2,6-DTP, or pyridine) increased with increasing DPE of the [POM]−n-donor complex, with the exception of the barrier over the [POM]−2-butanol cluster, which was similar to that over the [POM]−water cluster

$$\begin{aligned}&\text{butanol (136 kJ mol}^{-1}\text{)} \approx \text{water (137 kJ mol}^{-1}\text{)} <\\ &\text{2,6-DTP (unprotonated) (138−141 kJ mol}^{-1}\text{)} <\\ &\text{pyridine (146 kJ mol}^{-1}\text{)} <\\ &\text{2,6-DTP (unprotonated) (153−156 kJ mol}^{-1}\text{)}\end{aligned} \quad (9)$$

The calculated changes in adsorption strengths and activation barriers are slightly smaller (<10 kJ mol^{-1}) than those caused by changes in the identity of the central or addenda atom in POM clusters.

The calculations reported herein indicate that the interactions between the POM and the support, other POM structures, or coadsorbates all increase deprotonation energies, as well as elimination activation barriers, when the interacting species acts as a proton acceptor. At first glance, this might appear to be at odds with data that show weak effects of POM surface density on the resulting values of k_2 and K_4. It is unlikely that POM clusters are entirely isolated, as they can interact with the support, form POM surface arrays, or bind gas-phase coadsor-

bates. All of these interactions increase both the deprotonation energy and the elimination activation barrier and result in weaker alcohol adsorption as a result of charge transfer from these external "ligands" to the anionic cage of the POM structure. Although each of these ligands results in different DPE values and corresponding elimination barriers as compared to the bare POM, the changes in the DPEs and elimination barriers between different ligands (support, POM, and coadsorbates) are rather small. Under actual reaction conditions, n-donor molecules are always present and as such interact with all of the free acid sites which weaken the influence of these interactions further. As a result, POM–POM, POM–support, and other adsorbate – POM interactions may go undetected. This is in agreement with experimental results that show little influence of variations in the POM surface density on the rate.[10]

We have focused herein predominantly on the adsorption of various ligands (POSS, other POM clusters, and n-donors) onto one of the protons of the reactive POM cluster. The ligands examined, however, can also reorient their positions and act as proton donors, which is energetically less favorable than acting as a proton acceptor. This would result in the exact opposite trends because they would extract electron density from the POM cluster and thus lower the DPE, increase the alcohol adsorption, and decrease the elimination activation energies. Although these ligands are better proton acceptors, the greater availability of the oxygen sites compared to the number of protons on the POM clusters would likely increase the number of proton-donating interactions with the POM, thus potentially balancing out the increase in DPEs and elimination barriers that result from the proton-accepting interactions. This would be consistent with the insensitivity of the experimental results to changes in these ligands.

3.7. Effect of Cation Substitution. The partial replacement of protons by large alkali cations alters the secondary POM structure and increases the exposed surface area.[6,11,50,51] The observed decrease in the enthalpy of adsorption of ammonia and other polar molecules on alkali-substituted Keggin structures[50] appears to reflect a decrease in acid strength upon cation substitution. The adsorption of alkali cations can therefore alter the acid strength of primary Keggin structures and their catalytic properties. To probe this effect, we examined the deprotonation of $NaH_2PW_{12}O_{40}$, $CsH_2PW_{12}O_{40}$, and $CsH_2PW_{12}O_{40}$ structures, in which one of the protons in $H_3PW_{12}O_{40}$ was replaced by either a Na or a Cs cation. The presence of a Na cation increased DPE values from 1087 kJ mol^{-1} for the HPW Keggin unit to 1124 kJ mol^{-1}, consistent with a lower acid strength. 2-Butanol dehydration activation barriers concurrently increased from 132 to 145 kJ mol^{-1}. The substitution of one of the protons in $H_3PW_{12}O_{40}$ with Cs ($CsH_2PW_{12}O_{40}$) increased the DPE to 1157 kJ mol^{-1}. Similarly, the exchange of one of the protons in $H_3PMo_{12}O_{40}$ to form $CsH_2PMo_{12}O_{40}$ increased the DPE from 1107 to 1177 kJ mol^{-1}. As in the case of POSS and coadsorbate effects, the concurrent increase found for DPE and $E_{act}^{(2)}$ upon cation substitution reflects the increase in the electron density of the outer POM shell by the replacement of protons with less electropositive ligands. The calculated increase in DPE in replacing a proton in the POM cluster with Cs appears to be rather large, especially considering that Cs-substituted POM clusters are quite effective in catalyzing the dehydration reaction. The differences might arise from the coordination of other n-donors such as the alcohol or water to the Cs ion. This might also be due to the distribution of Cs that results from actual synthesis. $Cs_{2.5}$HPW, for example, might not correspond to aggregates with a uniform distribution of Cs cations and protons

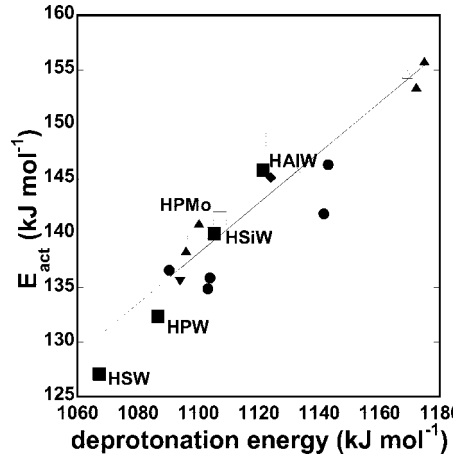

Figure 9. Activation barrier for 2-butanol dehydration plotted versus POM deprotonation energy for (■) various central atoms, (●) various coadsorbates on HPW, (▲) 2,6-di-*tert*-butylpyridine adsorbed to HPW with various adsorbed configurations, (▼) HPW with proton 2 moved from an O_c atom to an O_d atom, (♦) HPW with an Na countercation replacing proton 2, (Δ) HAlW with various coadsorbates, and (□) HPMo intact, partially decomposed and reduced species. Linear fit has a slope of 0.23 and an R^2 value of 0.85.

but rather to HPW supported on Cs_3PW, consistent with 2,6-di-*tert*-butylpyridine titration results that suggest higher proton concentrations at the surface of the $Cs_{2.5}$HPW crystallites than expected from a uniform distribution.[45] Interpretation of the experimental results of cation-exchanged POM clusters are, in general, ambiguous, as the overall rate constant of a catalyst with a nominal composition of $Y_xH_{3-x}PW$ (where Y is an exchange cation), for example, corresponds to the sum of the individual rate constants for H_3PW, YH_2PW, and Y_2HPW and their respective concentrations, which are, in most cases, experimentally inaccessible.

3.8. Correlations of 2-Butanol Dehydration Activation Barriers with Deprotonation Energies. The calculated adsorption and reaction energies and activation barriers reported herein specifically addressed how DPE values and catalytic rates depend on the (1) central atom, (2) addenda atom, (3) POM decomposition, (4) POM reduction, (5) interaction with supports, (6) inter-POM interactions, (7) presence of coadsorbates, and (8) substitution by alkali cations. The deprotonation energy emerges as an accurate descriptor for the effects of these structural and compositional changes on the adsorption energy of alcohol monomers and dimers and on the elimination activation barriers; the latter two influence the rates through K_4 and k_2, respectively (eq 3). In fact, these structural and compositional changes can all be described by a general linear correlation between elimination activation barriers ($E_{act}^{(2)}$) and DPE values (Figure 9) with a slope of 0.23. Changes in structure, composition, or reaction environment can then be treated as general ligand effects that influence dehydration rates on POM clusters through their concomitant effects on DPE values. The slope in the correlation of 0.23 is very close to the slope of 0.25 that arises from the Evans−Polanyi linear free energy relationship that relates the activation barrier to the heat of reaction. This falls out naturally from a thermodynamic cycle analysis (presented in the next section), which shows a direct relationship between the activation barrier and the heat of reaction for the heterolytic dissociation of the O−H bond.

3.9. Born−Haber Thermodynamic Cycle Analysis. The transition states for the E1 elimination reaction involve a cationic organic fragment interacting with an anionic POM structure. Gorte et al.[1−3,52,53] showed that a simple Born−Haber thermo-

SCHEME 3: Thermochemical Cycle for Formation of the Alcohol Dehydration Transition State over POM Acid Catalysts[a]

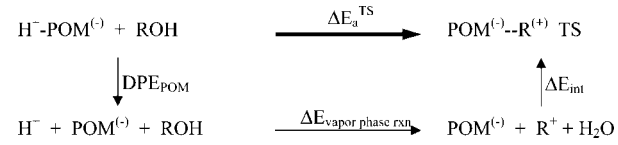

[a] Similar to scheme used in Aronson et al.[53]

chemical cycle can be used to assess the thermodynamic factors that determine the reactivity of solid acids. We used this approach previously[13] to examine the influence of adsorbate proton affinities, POM deprotonation energies, and the interaction energies of the ion pair on elimination activation barriers on POM clusters.

The formation of the elimination transition state can be dissected into a sequence of steps, as shown in Scheme 3, that involve deprotonation of the acid (DPE), transfer of the proton to the reactant ($\Delta E_{\text{vapor-phase rxn}}$), and formation of the cationic complex present in the ion pair with the anionic conjugate base (ΔE_{int}). These steps are reflected in the three terms in eq 10[13]

$$\Delta E_a^{TS} = \text{DPE} + \Delta E_{\text{vapor-phase rxn}} + \Delta E_{\text{int}} \qquad (10)$$

$\Delta E_{\text{vapor-phase rxn}}$ is defined as the reaction energy for proton transfer to the alcohol to form either a protonated alcohol [ROH(g) + $H^+ \rightarrow (ROH)^+$] or a carbenium ion together with water [ROH(g) + $H^+ \rightarrow R^+ + H_2O$]. The latter is the most relevant species, because elimination proceeds through a late transition state with significant carbenium-ion character. ΔE_{int} is the interaction energy between the gas-phase carbenium ion and water molecule ($R^+ + H_2O$) and the POM anion of the ion pair in the transition state. We have assumed here that electronic energies can be used in place of enthalpies, thus neglecting corrections for zero-point energies in the analysis.

The structure of the alcohol reactant, and specifically the degree of substitution at its C_α carbon, has the strongest influence on E1 elimination barrier, because of a direct stabilization of the local positive charge at the cationic organic species in the transition state.[13] The $\Delta E_{\text{vapor-phase rxn}}$ term for the gas-phase part of the thermochemical cycle does not depend on the POM composition or on adsorbate-induced changes in POM properties. If only DPE were relevant in the POM-mediated part of this cycle, then ΔE_a^{TS} would be strictly proportional to DPE (with a slope of unity). In general, however, ΔE_{int} becomes more negative as the deprotonation energy (DPE) increases. This reflects the prediction from acid−base theory that stronger acids (HA) lead to weaker conjugate bases (A^-) upon deprotonation. Weaker conjugate bases are thus less effective in stabilizing the organic cation via electrostatic interaction in the ion pair that forms at the transition state. These two opposite consequences of acid strength lead to the observed compensation effects, in which the lower DPE (first term in eq 10) also leads to the formation of a less stable ion pair (third term in eq 10) as the protonated organic fragment returns to the proximity of the anionic cluster.[1−3] The variation in the stabilization of the ion pair is always smaller than that in the DPE. The elimination activation energies, therefore, decrease with decreasing DPE values and increasing acid strength, and the stabilization interaction at the transition state concurrently becomes weaker for the stronger acid.

Whereas the elimination barrier $E_{act}^{(2)}$ decreases with increased acid strength (smaller DPE), the dimer formation energy increases, leading to stronger inhibition effects by alcohol reactants or other n-donors. The rates as shown in eq 3 are thus controlled by the rate constant for elimination, the dimer formation equilibrium constant, and the prevalent alcohol pressure. At high alcohol pressures, the apparent rate constant becomes k_2/K_4. Because both $E_{act}^{(2)}$ and ΔH_{dimer}, depend linearly on the DPE, they compensate one another in the apparent activation energy measured under these conditions.

The results for POM clusters with different compositions reported in Table 4 show that any changes in composition that allow the POM to delocalize and stabilize the negative charge that forms in the anionic shell upon deprotonation act to decrease the elimination activation barriers but also to increase the stability of the dimer. The dimer formation energies, on the other hand, become weaker as the valence of the central atom decreases. This compensates for the increase in the elimination activation barriers during elimination reactions at higher alcohol pressures.

All proton-accepting ligands in the POM cluster, which include the support, neighboring POM clusters, coadsorbates, or compensating cations, such as Na^+ and Cs^+, increased the charge transferred into the oxide shell, which concurrently increased deprotonation energies and destabilized both cationic transition states and unreactive dimers. The increase in DPE decreases both the elimination rate constant (k_2) and the dimer formation constant (K_4), two terms that have opposite effects on dehydration rates. This leads to compensation effects, whereby any changes that decrease the DPE or increase the acid strength and thus increase elimination rate constants also lead to more stable unreactive dimers and to a decrease in dehydration rates. Our focus here has been on the proton-donating effects of these ligands. As proton acceptors, these ligands show the exact opposite effect, as they decrease the charge in the resulting POM anion.

4. Summary and Conclusions

The results from first-principles density functional theory calculations were compared with kinetic parameters measured from rate data to probe the mechanism and the catalytic features that control the dehydration of alcohols on polyoxometalate acid catalysts. The reaction proceeds through an E1 mechanism where the C—O bond is heterolytically cleaved, resulting in the formation of an ion pair consisting of a carbenium ion closely associated with an anionic POM cluster. All attempts to isolate an E2 transition state led to a carbenium-ion E1-type transition state, suggesting that true, concerted E2 pathways are not possible. The calculated activation barriers and overall reaction energies for the E1 mechanism taken together with entropic considerations and experimental results show that the rate of dehydration over the POM clusters is kinetically controlled by the rate constant for the elimination step. The dehydration rate is inhibited by n-donor species, including the alcohol reactant as well as the water product, which react with accessible protons to form unreactive dimers.

The calculated activation barriers for different Keggin compositions are in good agreement with those determined experimentally. Increases in the deprotonation energy, which indicate a weaker acid strength, predict increases in the alcohol dehydration barrier along with increases in the dimer formation energy for changes in the POM composition, proton positions, oxidation state, coordination with alkali cations, and presence of proton-accepting coadsorbates. All of these features effectively transfer electron density into the oxide shell of the POM, thus reducing the ability of the resulting anion to stabilize the negative charge of the conjugate base. The deprotonation

energy thus provides a universal index that captures how changes in POM composition and environment change the activation barrier for the elimination step ($E_{act}^{(2)}$) as well as the dimer formation energies. The structure and degree of substitution of the alcohol have the greatest influence on the elimination barrier, as they stabilize the cation that forms in the transition state. The changes in POM composition and reaction environment tend to be secondary, because any changes to increase the acidity subsequently lower the stabilization of the transition state as weaker interaction energies compensate for the lower deprotonation energies. The same holds true for the alcohol reactants, but the compensation is less significant. Despite the compensation, the increase in acidity tends to win out. The overall rate, however, is a function of the elimination rate constant as well as the dimer formation equilibrium constant. All of the changes reported herein that result in lower intrinsic activation barriers, $E_{act}^{(2)}$, are partly compensated by an increase the dimer formation energies. The calculated decrease in the elimination activation barriers is stronger than the increase in the dimer formation energies.

Acknowledgment. E.I. and J.M. gratefully acknowledge support from the Chemical Sciences, Geosciences, and Biosciences Division, Office of Basic Energy Sciences, Office of Science, U.S. Department of Energy, under Grant DE-FG02-03ER15479. This research was performed in part using the Molecular Science Computing Facility (MSCF) in the William R. Wiley Environmental Molecular Sciences Laboratory, a national scientific user facility sponsored by the U.S. Department of Energy's Office of Biological and Environmental Research and located at the Pacific Northwest National Laboratory. Pacific Northwest is operated for the Department of Energy by Battelle. Resources administrated by the Information Technology & Communication Department at the University of Virginia and by the High Performance Computing Group at Pennsylvania State University were used in part to complete this study. We thank Professor R. J. Davis (University of Virginia) for helpful discussions.

References and Notes

(1) Corma, A. *Chem. Rev.* **1995**, *95*, 559.
(2) Farneth, W. E.; Gorte, R. J. *Chem. Rev.* **1995**, *95*, 615.
(3) Biaglow, A. I.; Gorte, R. J.; White, D. *J. Catal.* **1994**, *148*, 779.
(4) Misono, M.; Mizuno, N.; Katamura, K.; Kasai, A.; Konishi, Y.; Sakata, K.; Okuhara, T.; Yoneda, Y. *Bull. Chem. Soc. Jpn.* **1982**, *55*, 400.
(5) Mizuno, N.; Han, W.; Kudo, T. *J. Catal.* **1998**, *178*, 391.
(6) Okuhara, T.; Mizuno, N.; Misono, M. *Adv. Catal.* **1996**, *41*, 113.
(7) Macht, J.; Janik, M. J.; Neurock, M.; Iglesia, E. *Angew. Chem., Int. Ed.* **2007**, *46*, 7864.
(8) Janik, M. J.; Davis, R. J.; Neurock, M. *J. Catal.* **2006**, *244*, 65.
(9) Janik, M. J.; Campbell, K. A.; Bardin, B. B.; Davis, R. J.; Neurock, M. *Appl. Catal. A* **2003**, *256*, 51.
(10) Bardin, B. B.; Bordawekar, S. V.; Neurock, M.; Davis, R. J. *J. Phys. Chem. B* **1998**, *102*, 10817.
(11) Kozhevnikov, I. V. *Chem. Rev.* **1998**, *98*, 171.
(12) Okuhara, T.; Hu, C. W.; Hashimoto, M.; Misono, M. *Bull. Chem. Soc. Jpn.* **1994**, *67*, 1186.
(13) Macht, J.; Janik, M. J.; Neurock, M.; Iglesia, E. *J. Am. Chem. Soc.* **2008**, *130*, 10369.
(14) Ganapathy, S.; Fournier, M.; Paul, J. F.; Delevoye, L.; Guelton, M.; Amoureux, J. P. *J. Am. Chem. Soc.* **2002**, *124*, 7821.
(15) Lopez, X.; Bo, C.; Poblet, J. M. *J. Am. Chem. Soc.* **2002**, *124*, 12574.
(16) Fernandez, J. A.; Lopez, X.; Poblet, J. M. *J. Mol. Catal. A* **2007**, *262*, 236.
(17) Lee, K. Y.; Arai, T.; Nakata, S.; Asaoka, S.; Okuhara, T.; Misono, M. *J. Am. Chem. Soc.* **1992**, *114*, 2836.
(18) Janik, M. J.; Davis, R. J.; Neurock, M. *Catal. Today* **2005**, *105*, 134.
(19) Kresse, G.; Hafner, J. *Phys. Rev. B* **1993**, *47*, 558.
(20) Kresse, G.; Furthmuller, J. *Comput. Mater. Sci.* **1996**, *6*, 15.
(21) Kresse, G.; Furthmuller, J. *Phys. Rev. B* **1996**, *54*, 11169.
(22) Vanderbilt, D. *Phys. Rev. B* **1990**, *41*, 7892.
(23) Perdew, J. P.; Chevary, J. A.; Vosko, S. H.; Jackson, K. A.; Pederson, M. R.; Singh, D. J.; Fiolhais, C. *Phys. Rev. B* **1992**, *46*, 6671.
(24) Brown, G. M.; Noe-Spirlet, M. R.; Busing, W. R.; Levy, H. A. *Acta Crystallogr.* **1977**, *B33*, 1038.
(25) Mills, G.; Jonsson, H.; Schenter, G. K. *Surf. Sci.* **1995**, *324*, 305.
(26) Henkelman, G.; Jonsson, H. *J. Chem. Phys.* **2000**, *113*, 9978.
(27) Henkelman, G.; Uberuaga, B. P.; Jonsson, H. *J. Chem. Phys.* **2000**, *113*, 9901.
(28) Eckert, J.; Sewell, T. D.; Kress, J. D.; Kober, E. M.; Wang, L. L.; Olah, G. *J. Phys. Chem. A* **2004**, *108*, 11369.
(29) Janik, M. J.; Davis, R. J.; Neurock, M. *Catal. Today* **2006**, *116*, 90.
(30) Bader, R. *Atoms in Molecules: A Quantum Theory*; Oxford University Press: New York, 1990.
(31) Henkelman, G.; Arnaldsson, A.; Jonsson, H. *Comput. Mater. Sci.* **2006**, *36*, 354.
(32) Sanville, E.; Kenny, S. D.; Smith, R.; Henkelman, G. *J. Comput. Chem.* **2007**, *28*, 899.
(33) Keister, J. W.; Riley, J. S.; Baer, T. *J. Am. Chem. Soc.* **1993**, *115*, 12613.
(34) Makov, G.; Payne, M. C. *Phys. Rev. B* **1995**, *51*, 4014.
(35) Janik, M. J.; Bardin, B. B.; Davis, R. J.; Neurock, M. *J. Phys. Chem. B* **2006**, *110*, 4170.
(36) Knozinger, H.; Buhl, H.; Kochloefl, K. *J. Catal.* **1972**, *24*, 57.
(37) Yamaguchi, T.; Tanabe, K. *Bull. Chem. Soc. Jpn.* **1974**, *47*, 424.
(38) Noller, H.; Thomke, K. *J. Mol. Catal.* **1979**, *6*, 375.
(39) Delsarte, S.; Grange, P. *Appl. Catal. A: Gen.* **2004**, *259*, 269.
(40) Campbell, K. A.; Janik, M. J.; Neurock, M.; Davis, R. J. *Langmuir* **2004**, *21*, 4738.
(41) van Santen, R. A.; Neurock, M. *Molecular Heterogeneous Catalysis: A Conceptual and Computational Approach*; Wiley-VCH: Weinheim, Germany, 2006; p 474.
(42) Misono, M.; Okuhara, T.; Ichiki, T.; Arai, T.; Kanda, Y. *J. Am. Chem. Soc.* **1987**, *109*, 5535.
(43) Jensen, F. *Introduction to Computational Chemistry*; John Wiley & Sons: New York, 1999; p 429.
(44) Ziegler, T. *Chem. Rev.* **1991**, *91*, 651.
(45) Macht, J.; Iglesia, E. 2008. Unpublished results.
(46) Sadakane, M.; Steckhan, E. *Chem. Rev.* **1998**, *98*, 219.
(47) Ohtsuka, R.; Morioka, Y.; Kobayashi, J. *Bull. Chem. Soc. Jpn.* **1989**, *62*, 3195.
(48) Janik, M. J.; Davis, R. J.; Neurock, M. *J. Phys. Chem. B* **2004**, *108*, 12292.
(49) Janik, M. J.; Davis, R. J.; Neurock, M. *J. Am. Chem. Soc.* **2005**, *127*, 5238.
(50) Kozhevnikova, E. F.; Kozhevnikov, I. V. *J. Catal.* **2004**, *224*, 164.
(51) Misono, M. *Chem. Commun.* **2001**, 1141.
(52) Gorte, R. J. *Catal. Lett.* **1999**, *62*, 1.
(53) Aronson, M. T.; Gorte, R. J.; Farneth, W. E. *J. Catal.* **1986**, *98*, 434.

JP8078748